Continuation of standard cirrus reflectance product from the EOS Terra and Aqua MODIS to Suomi NPP VIIRS
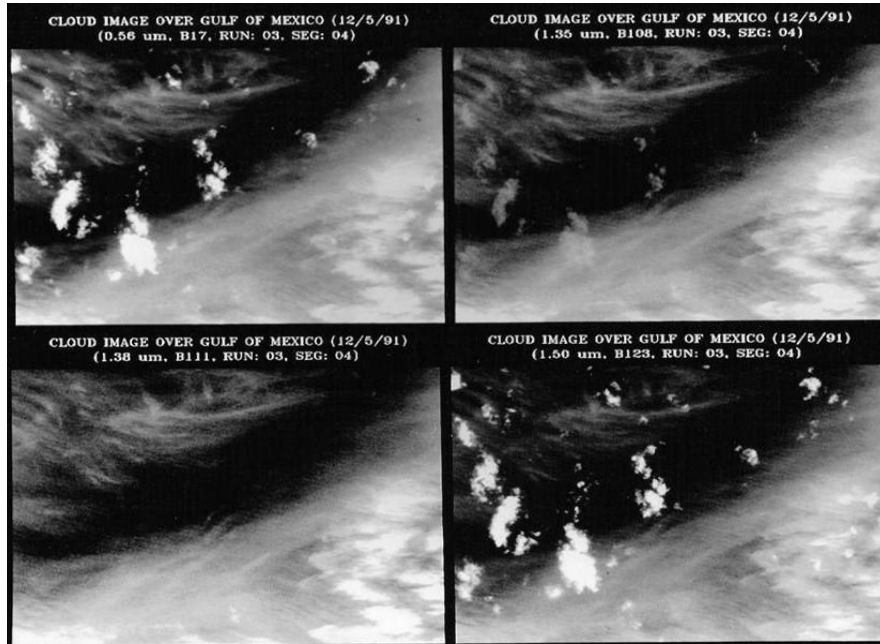
Bo-Cai Gao and Rong-Rong Li

May 2015

Remote Sensing Division,
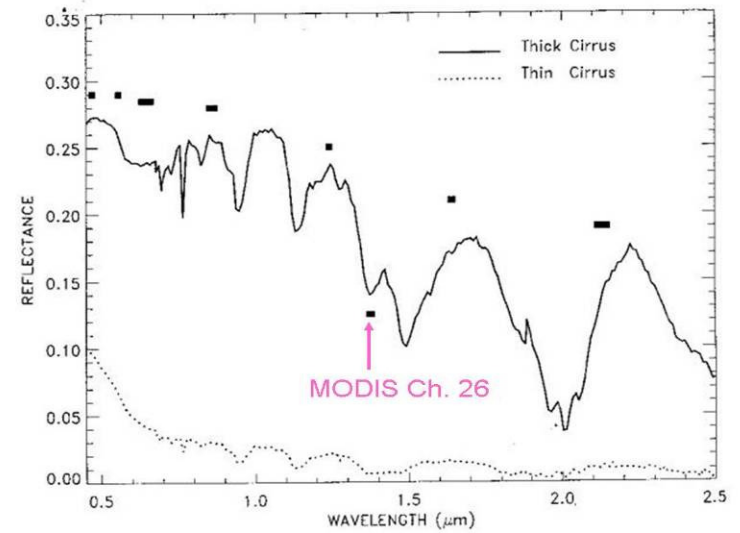Naval Research Laboratory, Washington, DC USA

INTRODUCTION

- Brief descriptions on MODIS and VIIRS cirrus detecting channels

- The cirrus reflectance algorithm

- Tasks performed till present

- Evaluation of VIIRS M9 channel & sample cirrus corrections

- Issues with VIIRS data - gain factors and horizontal striping

- Summary

Historical Development With MODIS 1.38-μm Cirrus Detecting Channel

Sample AVIRIS Images

CLOUD IMAGE OVER GULF OF MEXICO (12/5/91)
(0.56 um, B17, RUN: 03, SEG: 04)

CLOUD IMAGE OVER GULF OF MEXICO (12/5/91)
(1.35 um, B108, RUN: 03, SEG: 04)

CLOUD IMAGE OVER GULF OF MEXICO (12/5/91)
(1.38 um, B111, RUN: 03, SEG: 04)

CLOUD IMAGE OVER GULF OF MEXICO (12/5/91)
(1.50 um, B123, RUN: 03, SEG: 04)

Sample AVIRIS Cirrus Spectra & MODIS Channels

MODIS Ch. 26

MODIS Original RGB Image

1.38-μm MODIS Image

Cirrus-Corrected RGB Image
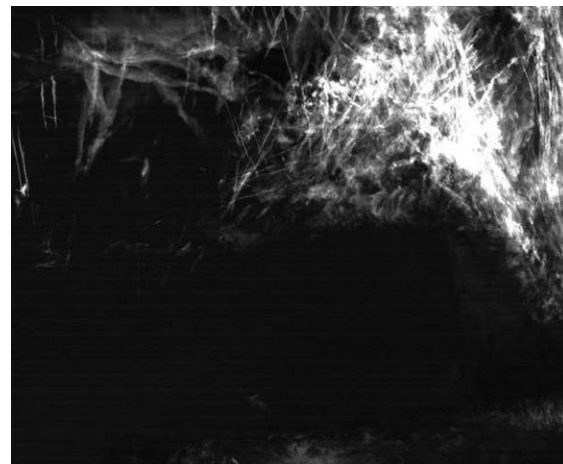
Equations for the Derivation of Cirrus Reflectances Using a scatter-plot approach & Cirrus Corrections

The apparent reflectance at the satellite level is defined as:

$$\rho^*_\lambda = \pi L_\lambda/(\mu_0 E_{0\lambda})$$

$$\rho^*_\lambda = \rho_{c\lambda} + T_{c\lambda} \rho_\lambda/(1 - S_{c\lambda} \rho_\lambda) \tag{1}$$

$\rho_{c\lambda}$: path radiance due to cirrus;

$S_{c\lambda}$: cloud scattering of upward radiation back to surface;

ρ_λ : Surface reflectance;

If $S_{c\lambda} << 1$, Eq. (1) becomes: $\qquad \rho^*_\lambda = \rho_{c\lambda} + T_{c\lambda} \rho_\lambda \tag{2}$

We found an empirical relation: $\qquad \rho_{c\lambda} = \rho_{c1.375}/K_a \tag{3}$

where K_a = Sun-cirrus-sensor vapor transmittance at 1.375 μm. It is derived empirically from a scatter plot.

Substituting Eq. (3) into (2), we get

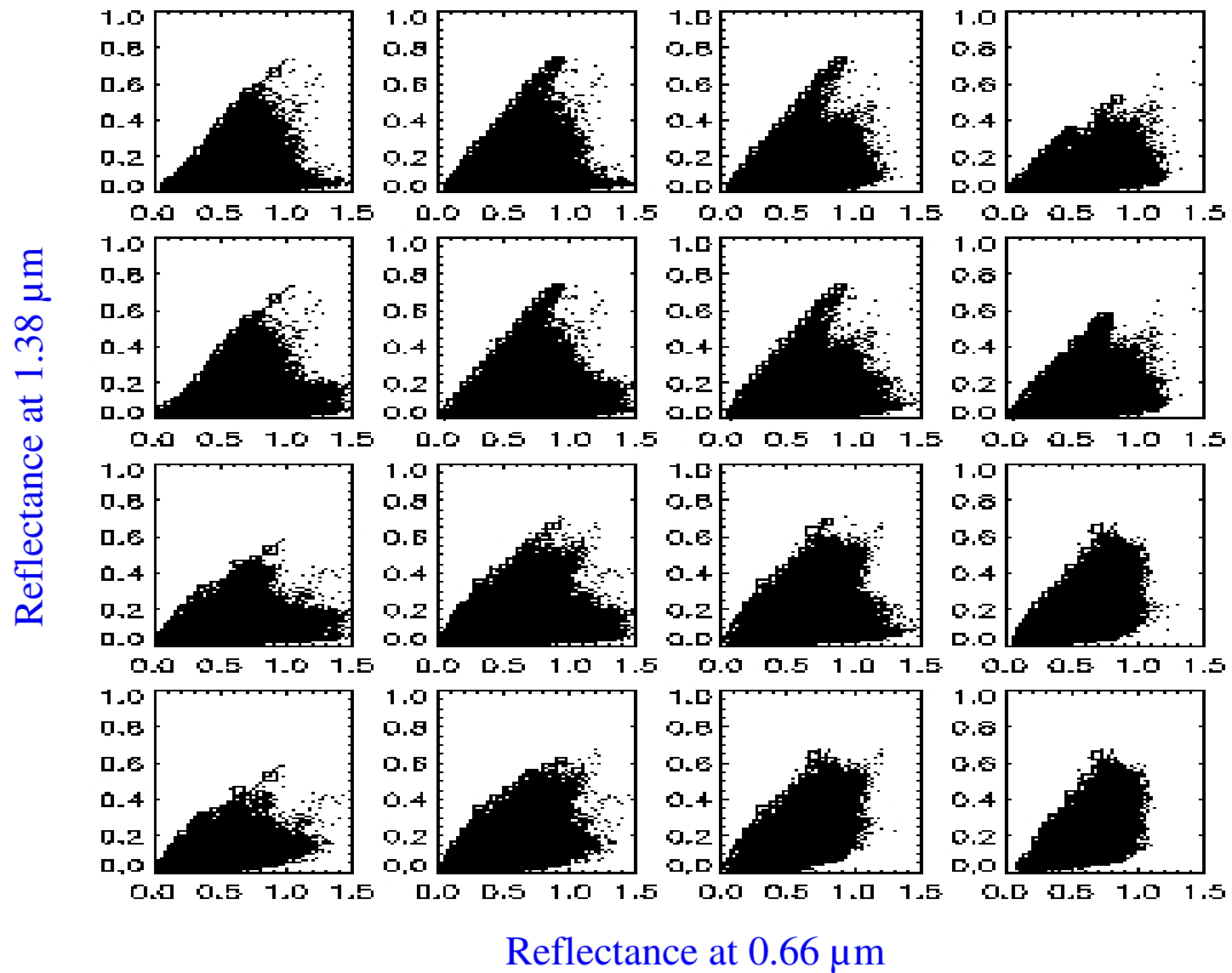$$T_{c\lambda} \rho_\lambda = \rho^*_\lambda - \rho_{c1.375}/K_a \tag{4}$$

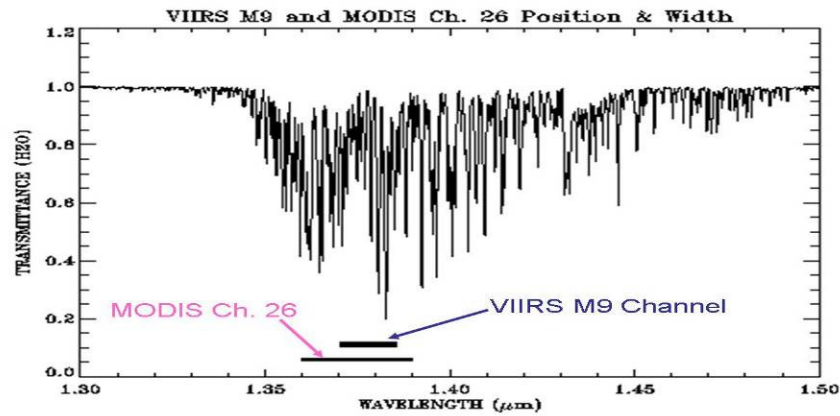To a good approximation: $\qquad T_{c\lambda} = 1 - \rho_{c\lambda}$

& $\qquad \rho_\lambda = (\rho^*_\lambda - \rho_{c1.375}/K_a)/(1 - \rho_{c1.375}/K_a) \tag{5}$
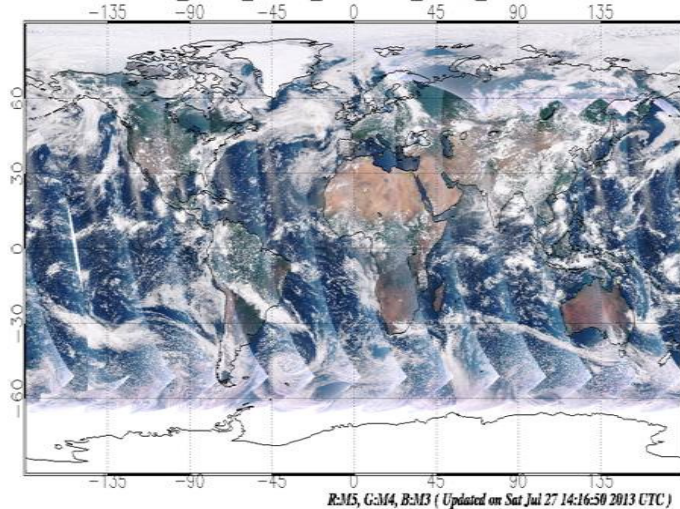
Estimates of the MODIS 1.375-µm Channel Water Vapor Transmittance by Dividing a large MODIS Scene into 4 x 4 Smaller Blocks

Reflectance at 1.38 µm
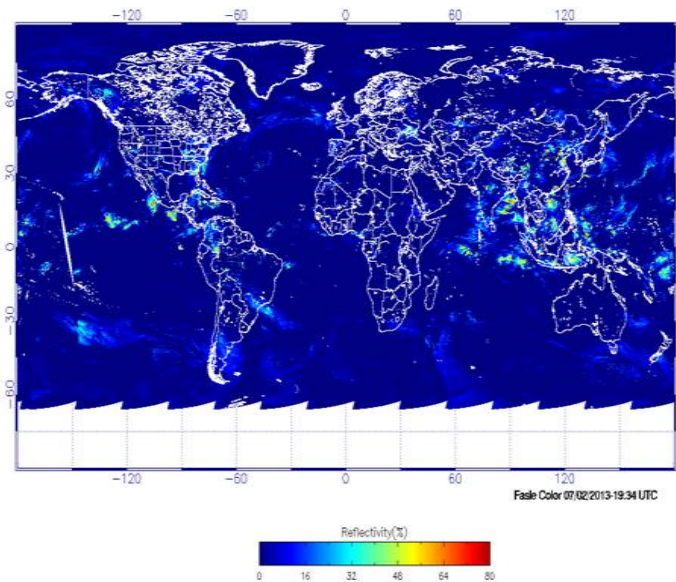
Reflectance at 0.66 µm

The VIIRS M9 Cirrus Detecting Channel (1.378 µm)

VIIRS M9 and MODIS Ch. 26 Position & Width

MODIS Ch. 26   VIIRS M9 Channel

(A) NPP_VIIRS_Global_TrueColor_Image_20130701

R:M5, G:M4, B:M3 (Updated on Sat Jul 27 14:16:50 2013 UTC)

(B) VIIRS_Global_Image_M9_20130701

Fasle Color 07/02/2013-19:34 UTC

Reflectivity(%)

We proposed to continue the cirrus reflectance data product from MODIS to VIIRS. The proposal was selected for funding.

Tasks Performed Till Present

- Obtained a copy of operational MODIS cirrus reflectance algorithm from a computer at University of Wisconsin in Madison.

- Modified the code so that it could be a standalone code (without MODI Toolkits) to run for a single MODIS granule.

- Developed IDL routines to extract VIIRS bands, solar and view angles, etc., from the VIIRS IFFSDR hdf file and to save as regular binary files.

- Re-structured and re-wrote major portions of MODIS code in Fortran 90 for VIIRS data processing. The code is now able to directly read in VIIRS binary data files, and produce VIIRS cirrus reflectance images and the M9 water vapor transmittance images (for water vapor molecules in the Sun-cirrus-sensor path).

- We were able to run, in batch mode, the VIIRS version of code for one day of data.

- At present, the output does not contain QA parameters and error and uncertainty estimates. The QA routines need to be developed and implemented in the future.

An Example of VIIRS Images Over Andes Mountains
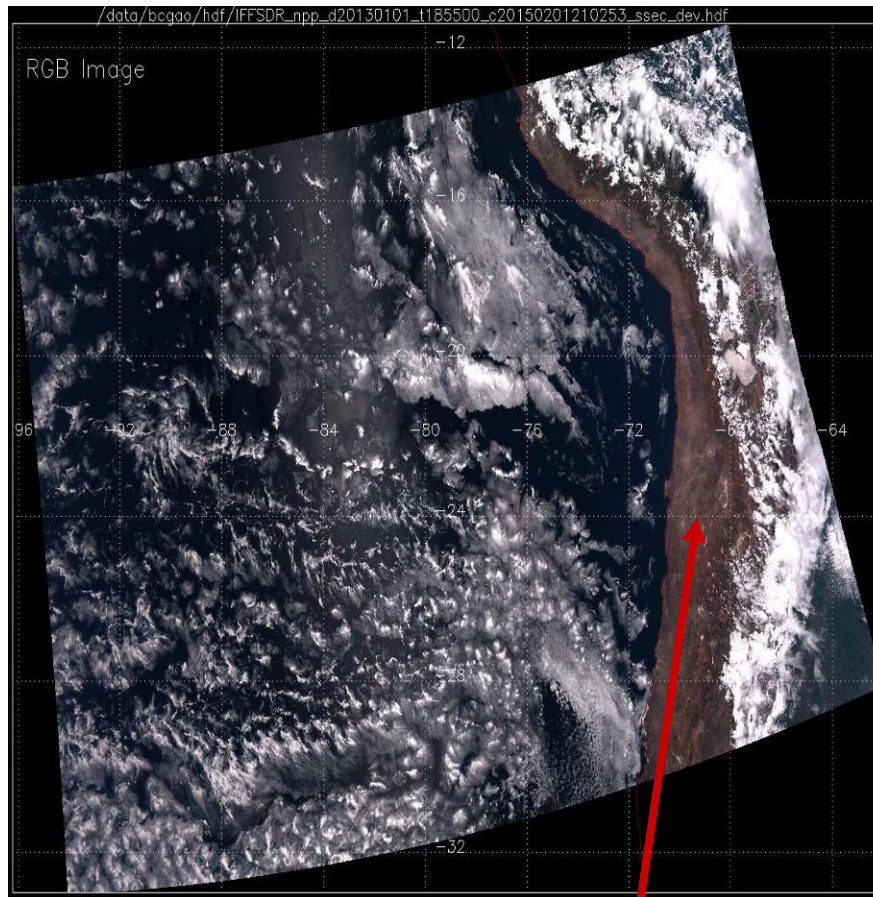
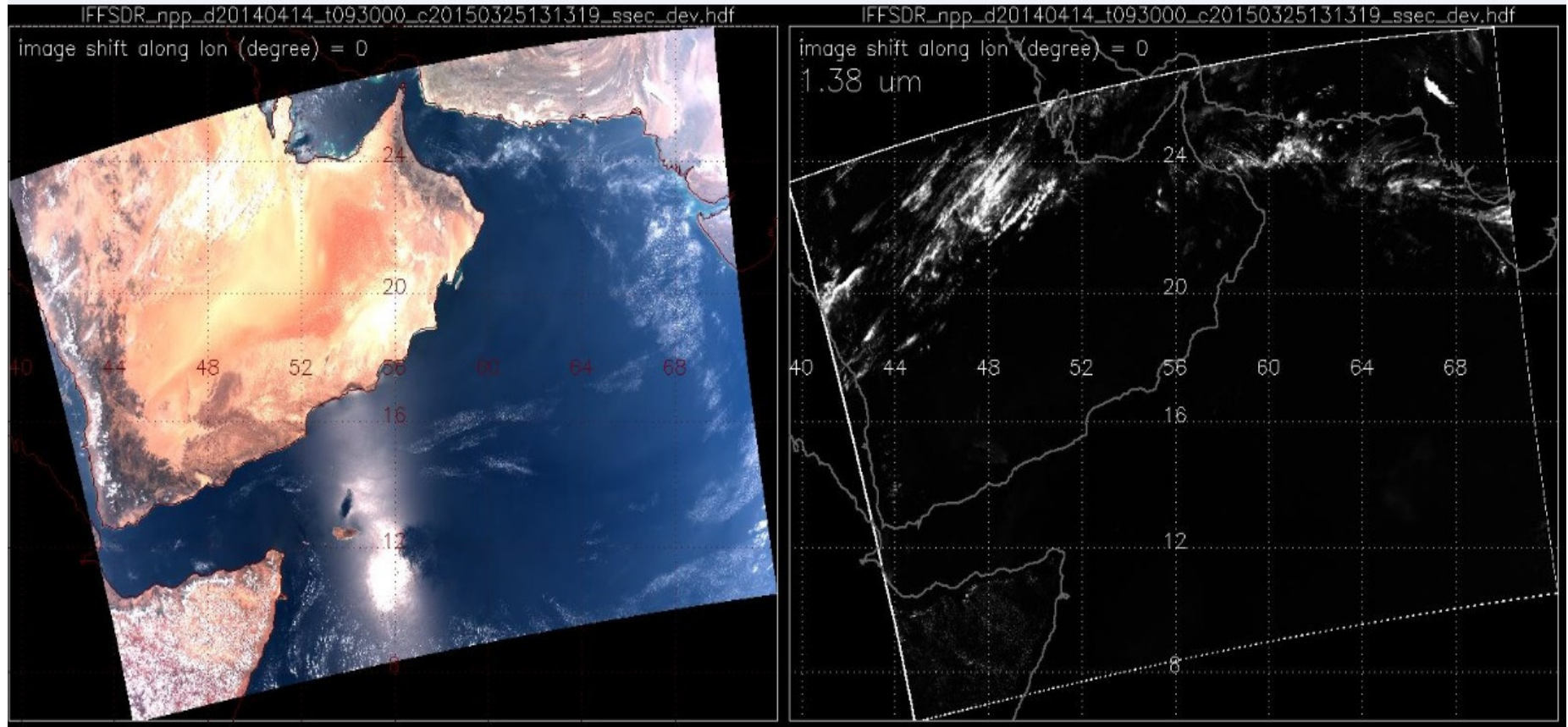VIIRS RGB Image   VIIRS M9 Image
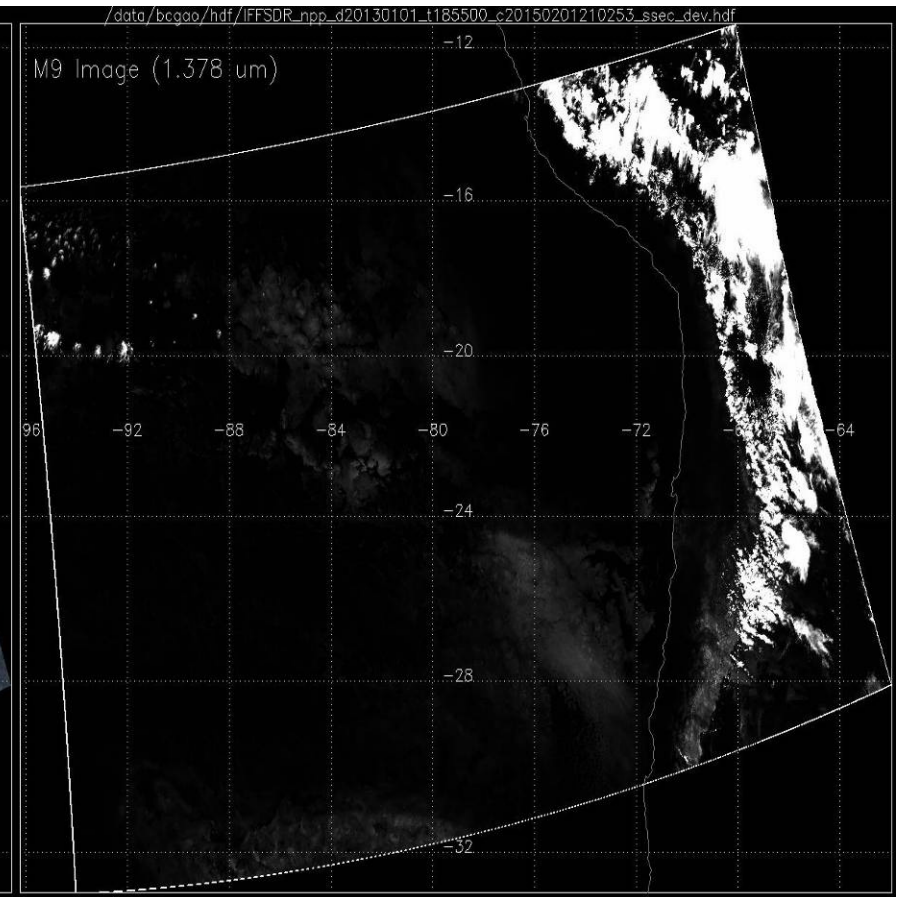
The high elevation mountains are not seen in the VIIRS M9 image.

8

An Example of VIIRS Images Over Desert & Sun glint Areas
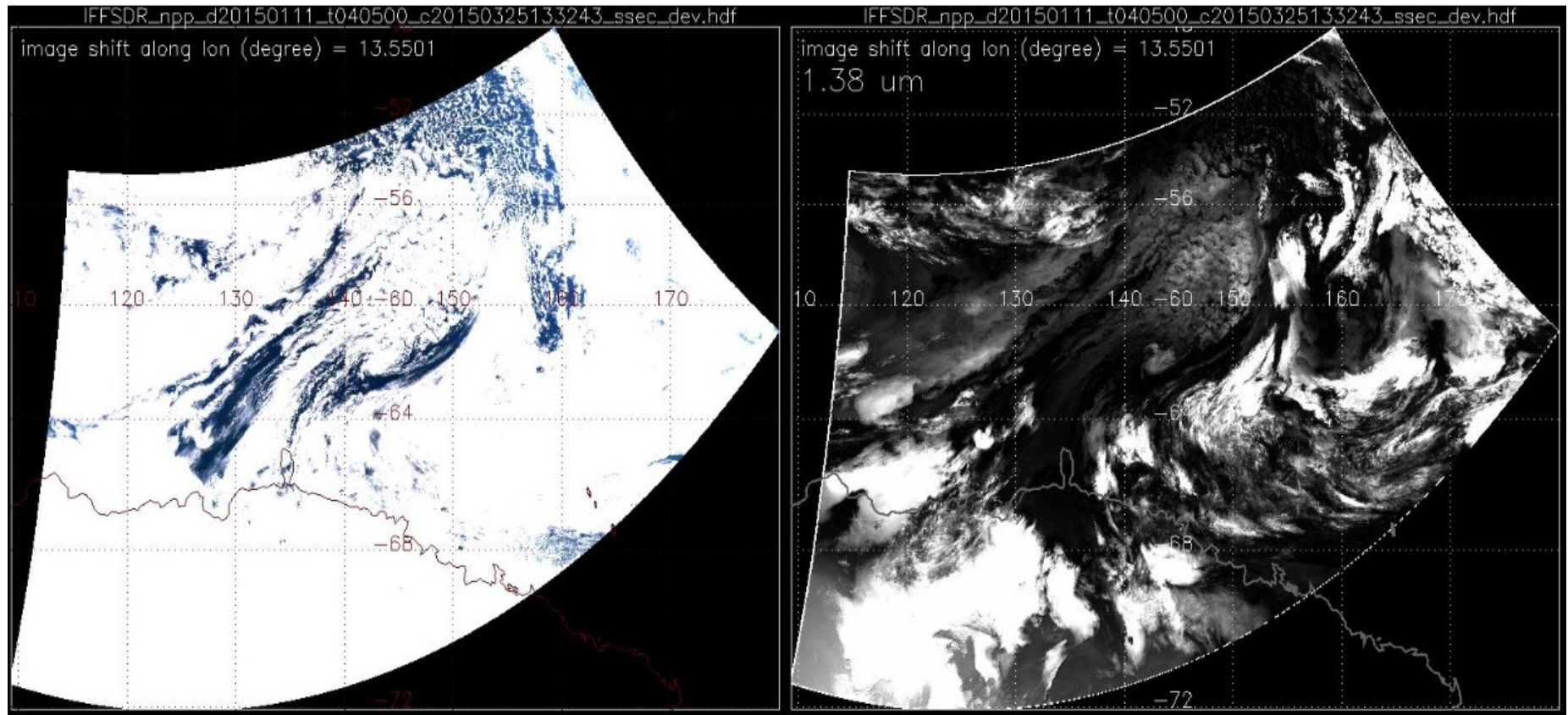
VIIRS RGB Image

VIIRS M9 Image

The VIIRS M9 image was not affected by reflection from desert and sunglint.

An Example of VIIRS Images Over High Latitude Regions
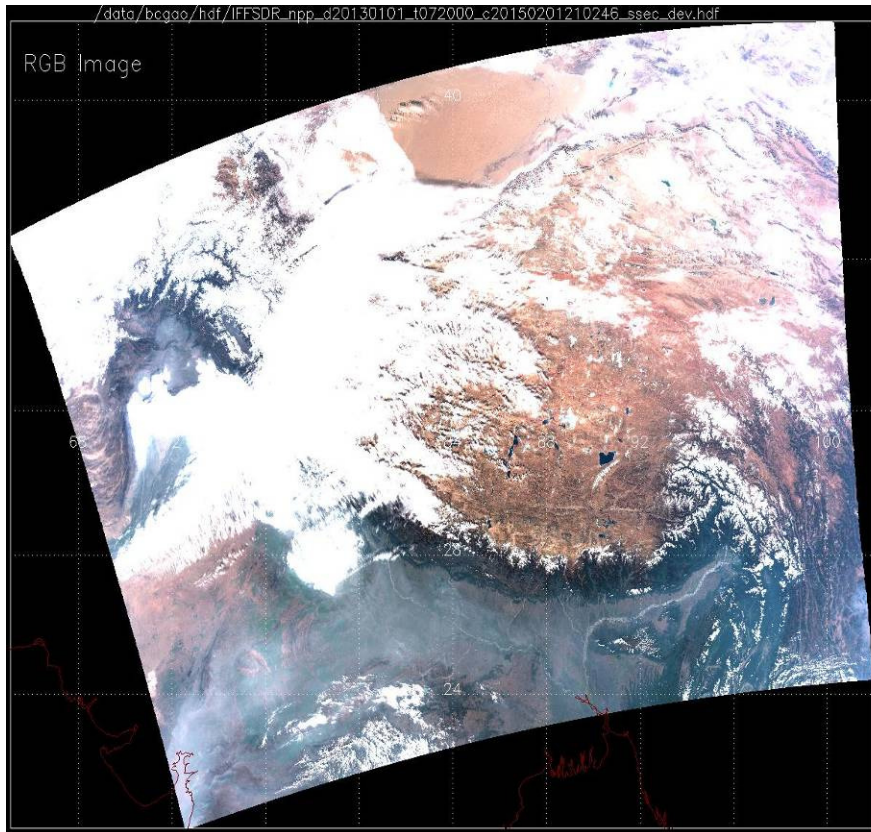
VIIRS RGB Image

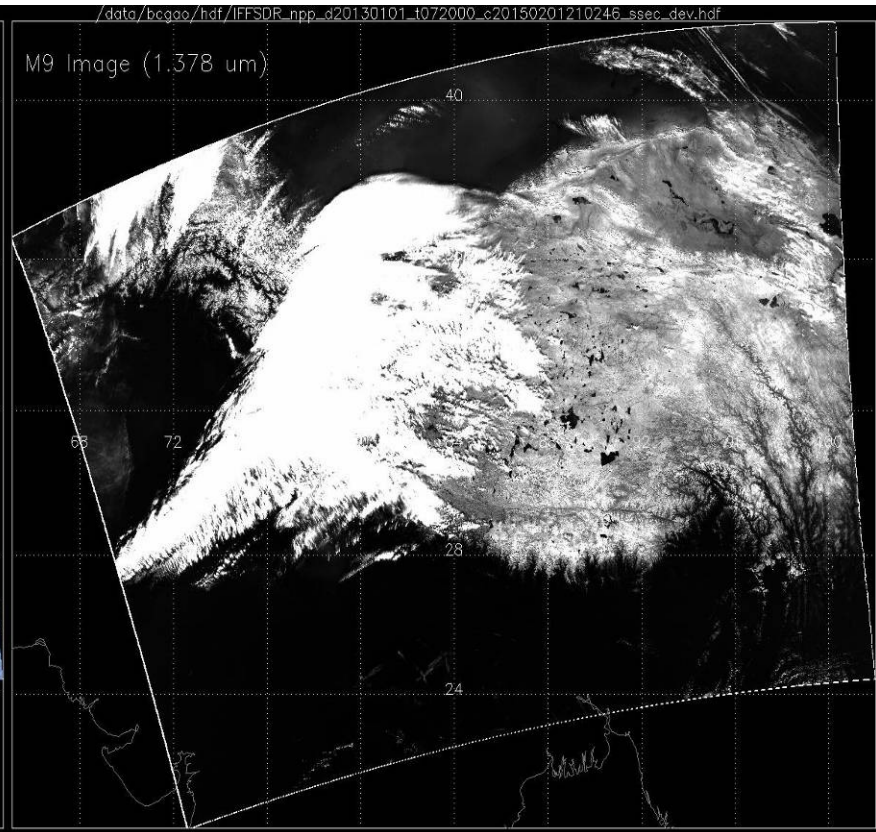**VIIRS M9 Image**

The VIIRS M9 image is very effective in detecting clouds in high latitude regions.

An Example of VIIRS Images Tibet Plateau

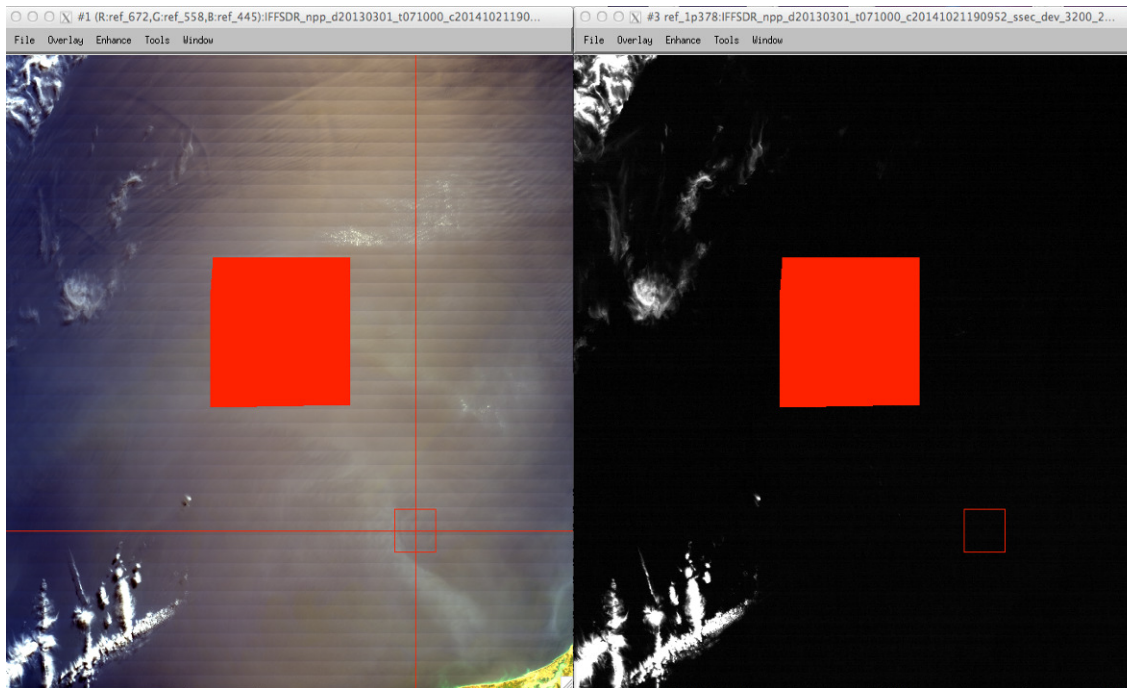VIIRS RGB Image   VIIRS M9 Image

The VIIRS M9 image is contaminated by surface reflection over Tibet under very dry atmospheric conditions.

Noise Estimation from the VIIRS M9 Band Image
(The estimated M9 band noise level ~ 0.00016 in reflectance unit)

VIIRS RGB Image

VIIRS M9 Image

The area in solid red color has no thin cirrus. The mean and standard deviation for each of VIIRS M1 – M11 bands over the area are calculated.

Filename: /sgi/VIIRS_Cirrus_Refl_Algorithm_2015/VIIRS_IDL_Readers_
ROI: Region #1 [Red] 28481 points

| Basic Stats	Min	Max	Mean	Stdev
Band 1	0.173803	0.184034	0.178254	0.001489
Band 2	0.143526	0.154025	0.148444	0.001607
Band 3	0.116447	0.126385	0.121817	0.001776
Band 4	0.085144	0.095423	0.090714	0.002029
Band 5	0.063314	0.075645	0.070277	0.002617
Band 6	0.056624	0.069956	0.064261	0.002854
Band 7	0.051228	0.065878	0.059481	0.003158
Band 8	0.041778	0.058211	0.050620	0.003561
Band 9	0.000000	0.001172	0.000570	0.000160
Band 10	0.037847	0.054793	0.047024	0.003716
Band 11	0.028544	0.042486	0.035880	0.003039

Conclusion: The VIIRS M9 band noise is really small. This band is directly usable for the removal of thin cirrus scattering effects in other VIIRS bands, without introducing noticeable noises into cirrus-corrected images.

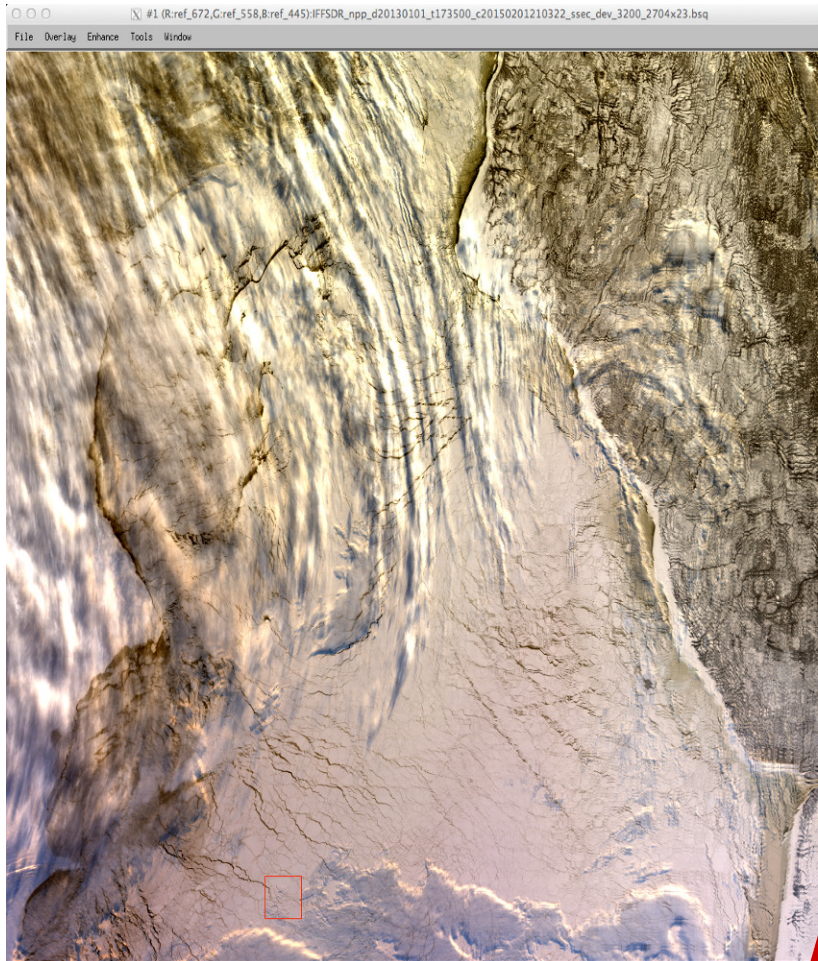# An Example of Cirrus Detection & Cirrus Removal Over Red Sea

VIIRS RGB Image   **Cirrus Reflectance Image**   **Cirrus-Removed RGB Image**
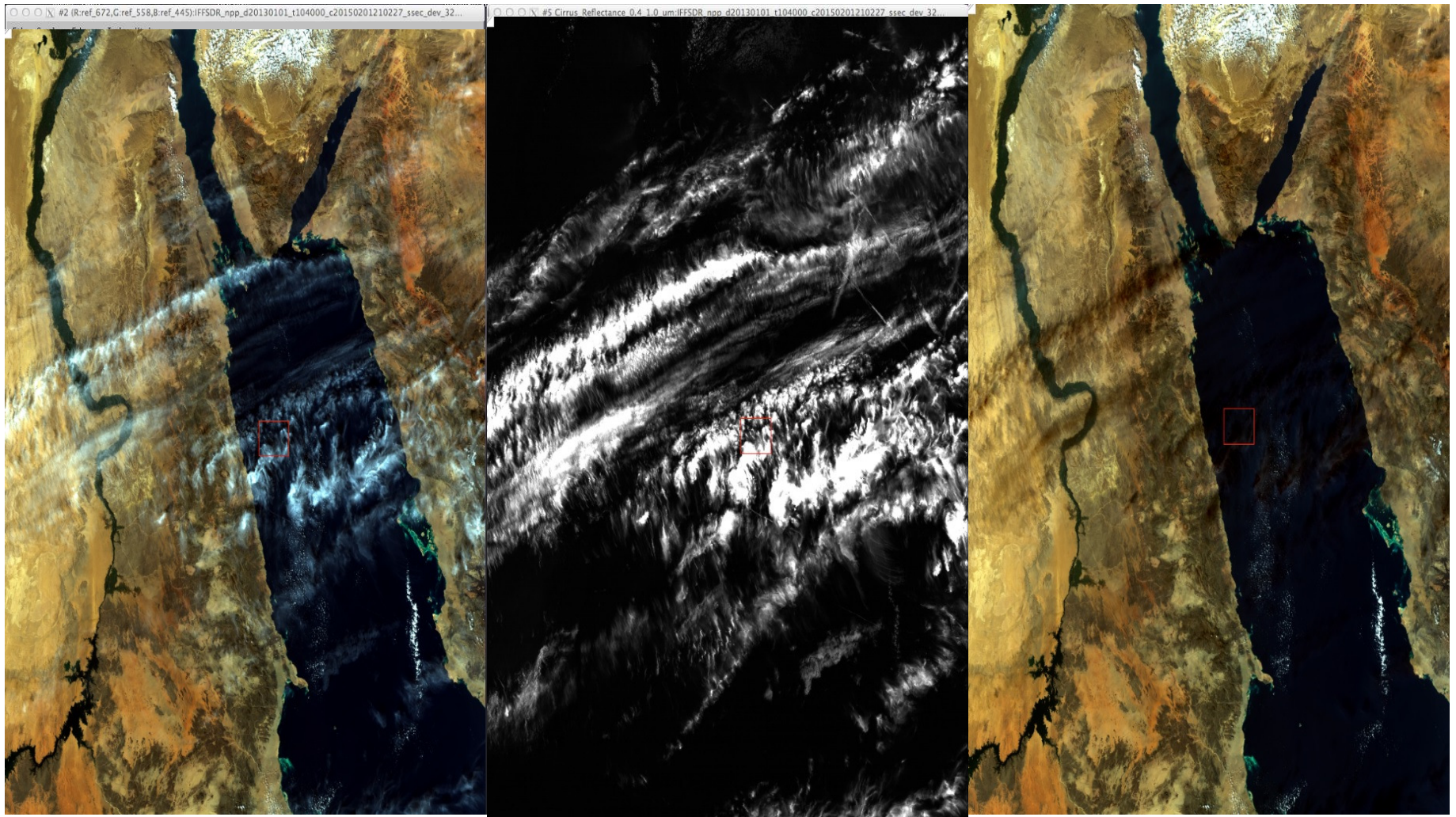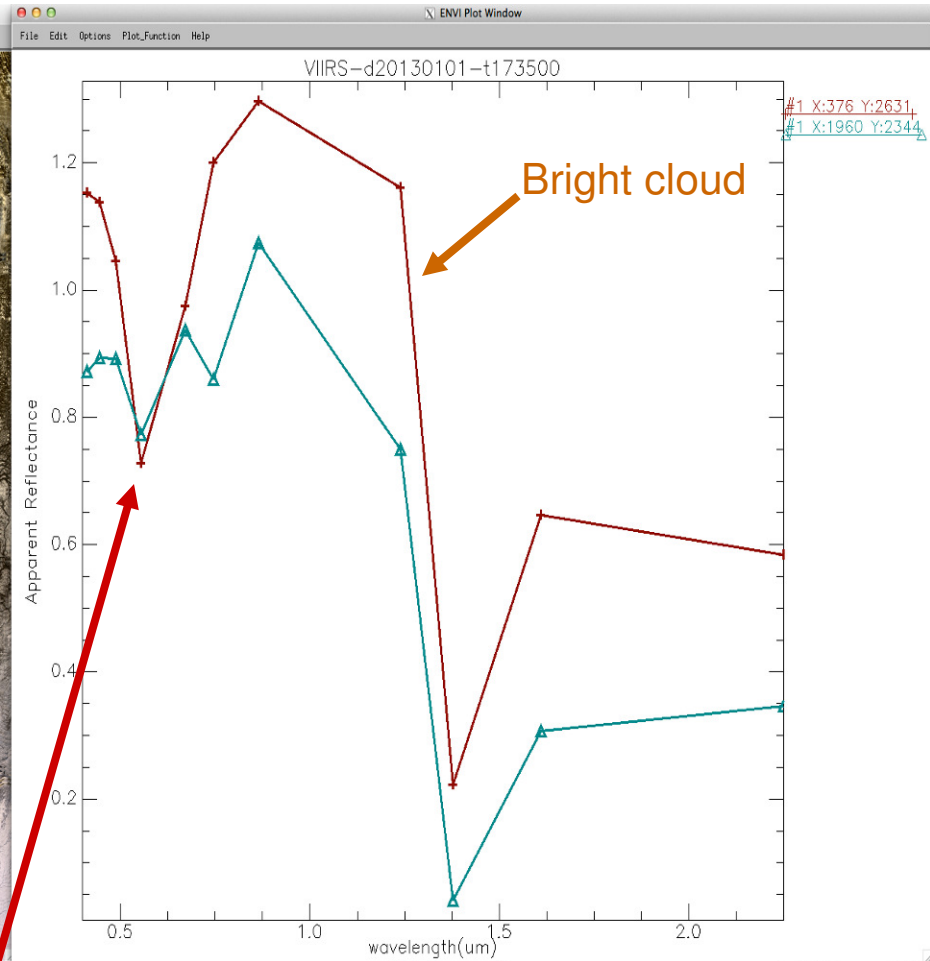
Issues with VIIRS Radiometric Calibrations

VIIRS RGB Image
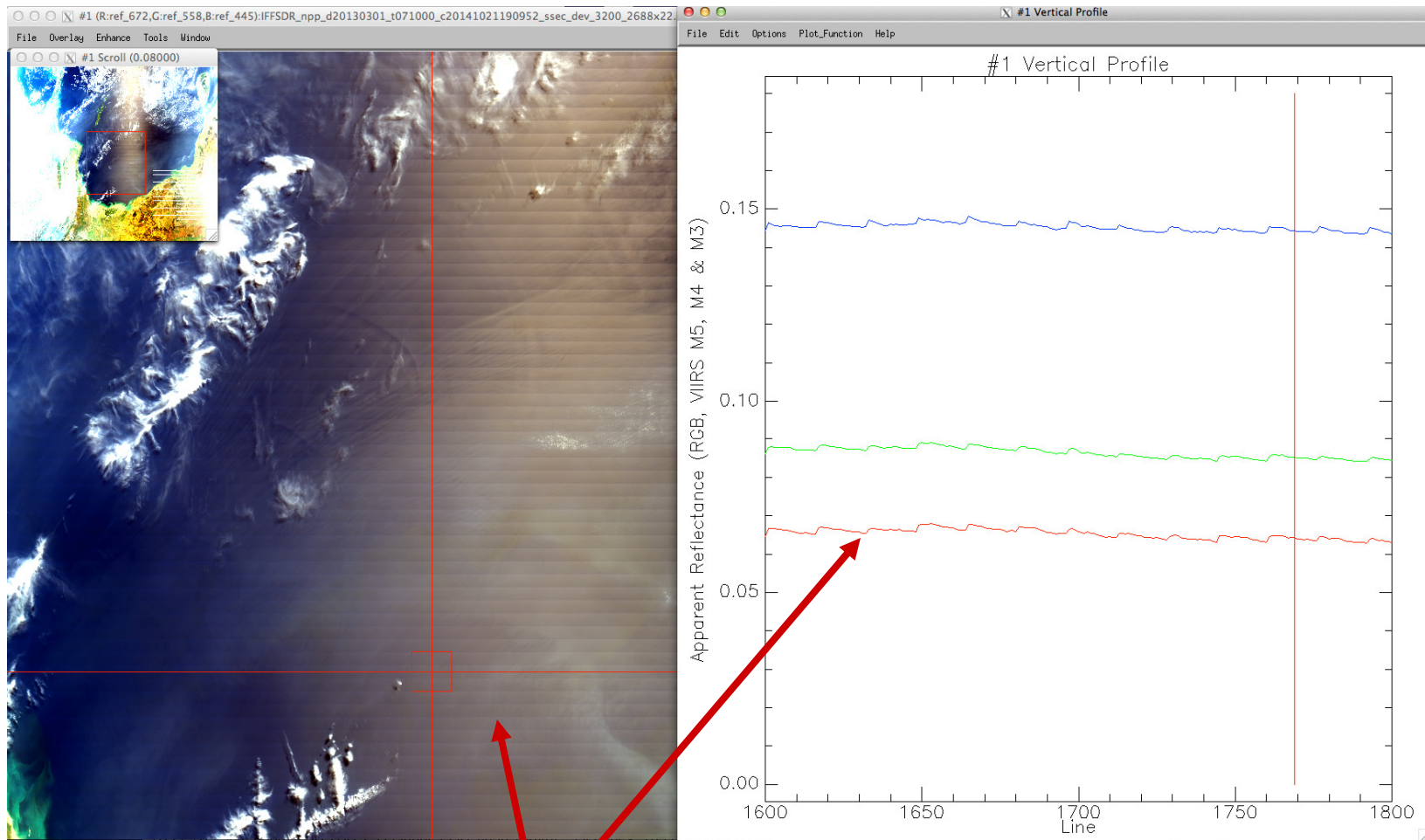
Apparent Reflectance vs Wavelength

The gain factor for VIIRS M4 band over bright target seems to be too small.

Issues with VIIRS Radiometric Calibrations (Continued)

VIIRS RGB Image

Vertical Profiles for VIIRS RGB Bands & for X = 1700 (near the imaging center)

- Horizontal striping in a number of VIIRS band images

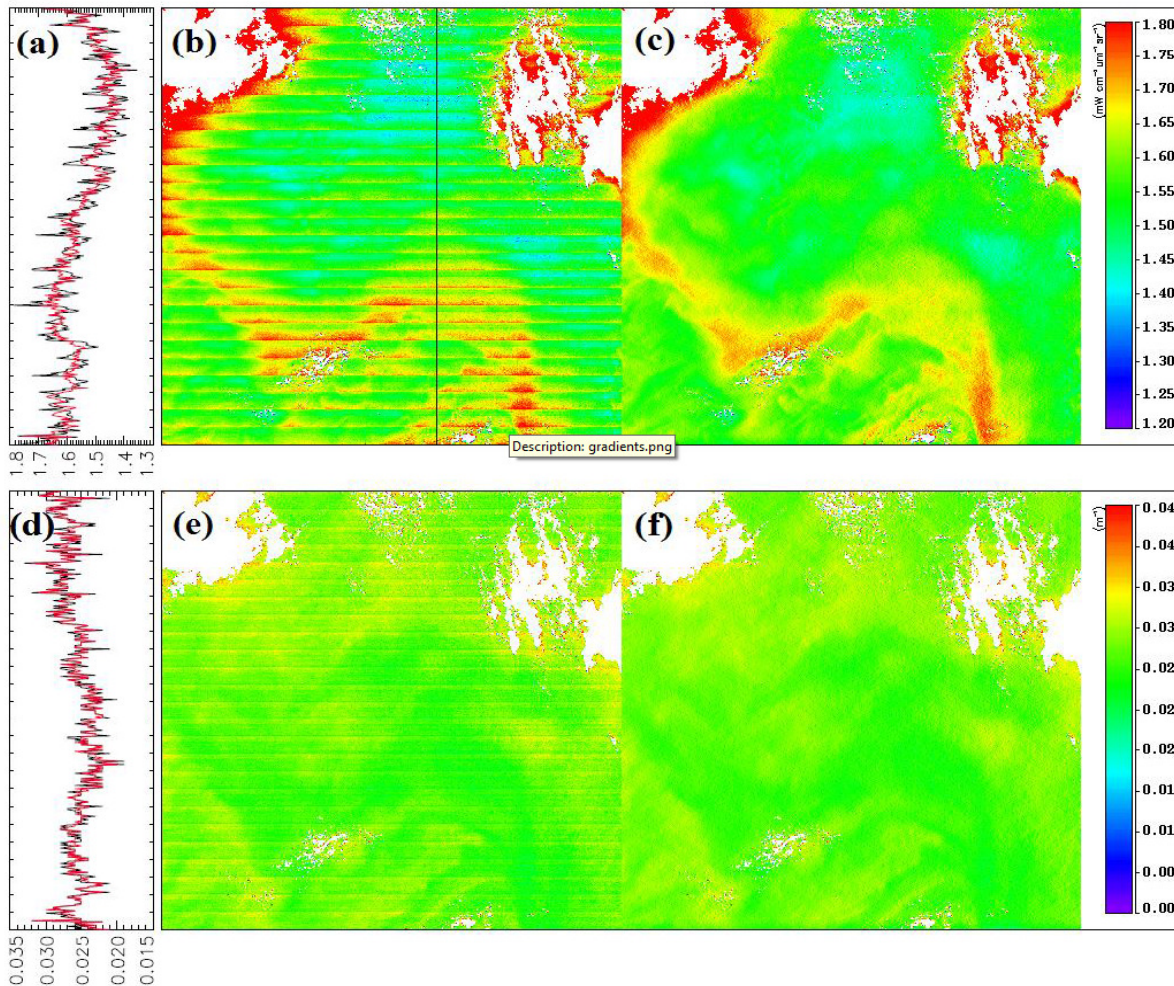# Effects of VIIRS Striping on Ocean Color Retrievals

Fig. 3. Destriping of ocean color products $nL_w(412)$ (upper panels: (a)–(c)) and diffuse attenuation coefficient $K_d(490)$ (lower panels: (d)–(f)) obtained from VIIRS-SNPP on April 19, 2014 at around 21:20 UTC near (13°S, 114°W). The original data are shown in panels (b) and (e), while the destriped data are shown in panels (c) and (f). The values along the black line in panel (b) are plotted in panels (a) and (d) with black lines from original images (panels (b) and (e)) and red lines from destriped images (panels (c) and (f)).

Due to striping in VIIRS SDR images, NOAA scientists have relied on spatial smoothing to improve the ocean color imagery (OE.22.028058).

It is highly desirable to first fix the striping problem in VIIRS SDR data products prior to make retrieval of ocean color data products.

SUMMARY

- The VIIRS M9 band is a well built band. It is very sensitive for thin cirrus detections with a noise level of about 0.00016 in reflectance unit. Unlike the corresponding MODIS band 26, VIIRS M9 is free of the thermal radiation leaking problem due to the addition of a blocking filter. Because of very low noise level, the VIIRS M9 data can be used directly for correction of thin cirrus scattering effects in other VIIRS bands below 2.25 micron.

- We have developed a preliminary and functional VIIRS cirrus reflectance algorithm. We now output the cirrus reflectances (valid for the 0.4 – 1.0 micron spectral range) and the upper level Sun-cirrus-sensor M9 band water vapor transmittances. The upper level water vapor transmittances can be useful for climate research in the future.

- We have identified several issues with VIIRS radiometric calibrations, such as gain factors, horizontal striping, and differential polarization. These issues should, in principle, be further addressed by VIIRS calibration scientists in different organizations.

Differential Polarization Among 16 Detectors of a Given VIIRS Band

The effect was previously reported by Guenther et al. in IGARSS 2011.

However, the effect was barely mentioned in the recent pre-launch VIIRS calibration paper. The relevant paragraph is (from TGRS.2014.2357678):
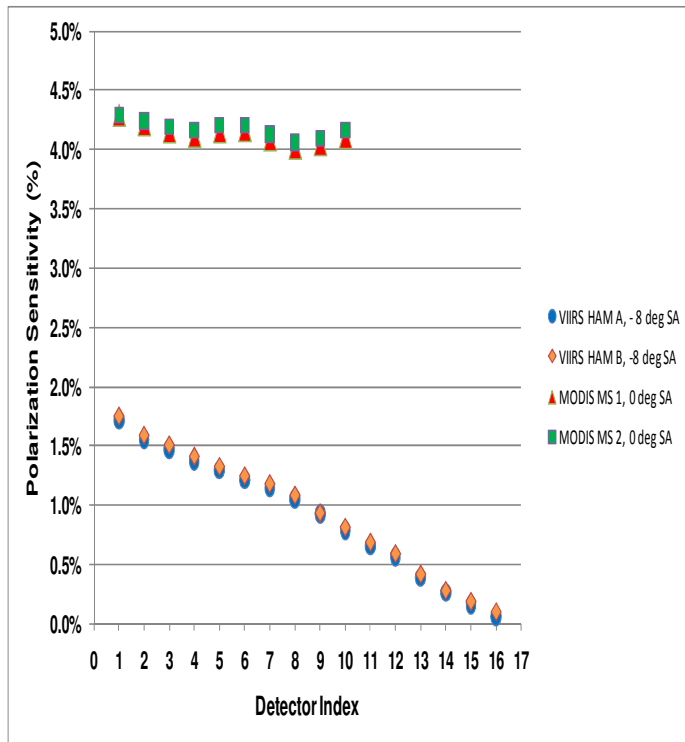

Fig. 4a. 0.412 um DoLP by detector for VIIRS at -8 scan angle and MODIS at 0 degrees scan angle.
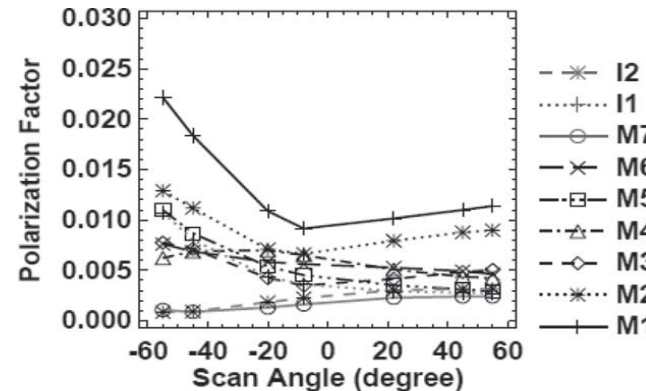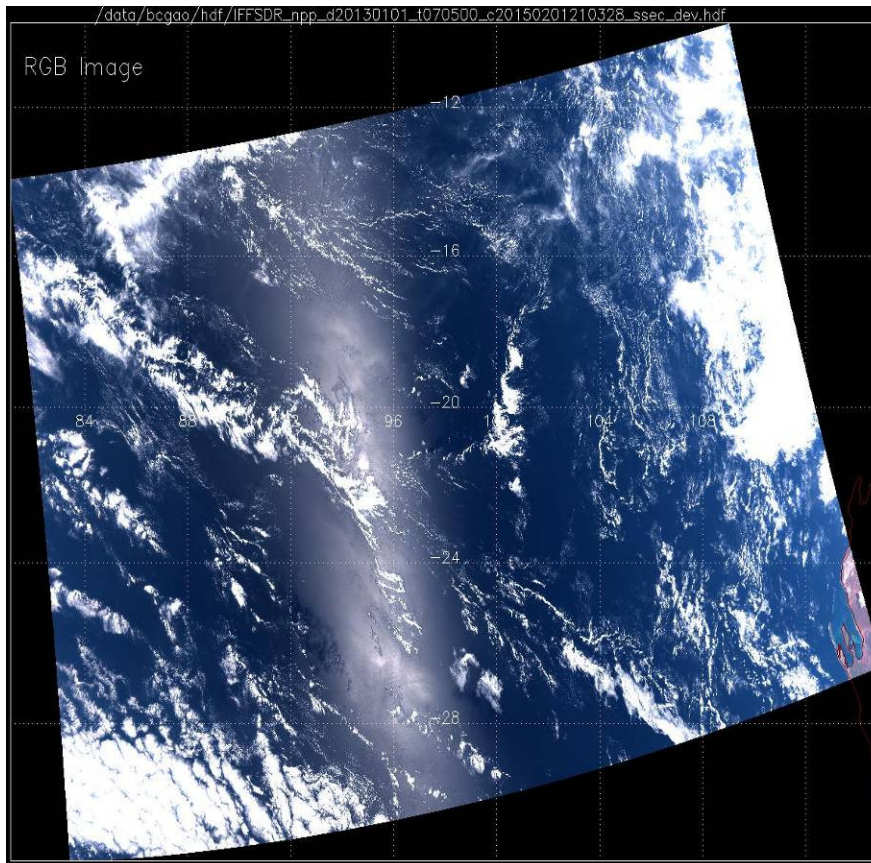

Fig. 8. VIIRS polarization for the VisNIR bands measured at seven angles.

Polarization: The two-cycle amplitudes determined from the polarization sensitivity testing are plotted in Fig. 8 as a function of the scan angle for all VisNIR bands (band-averaged HAM side A). The polarization measurements had shown very high repeatability, and the uncertainty due to repeatability was smaller than 0.15% for all VisNIR bands. The largest polarization sensitivity occurred in b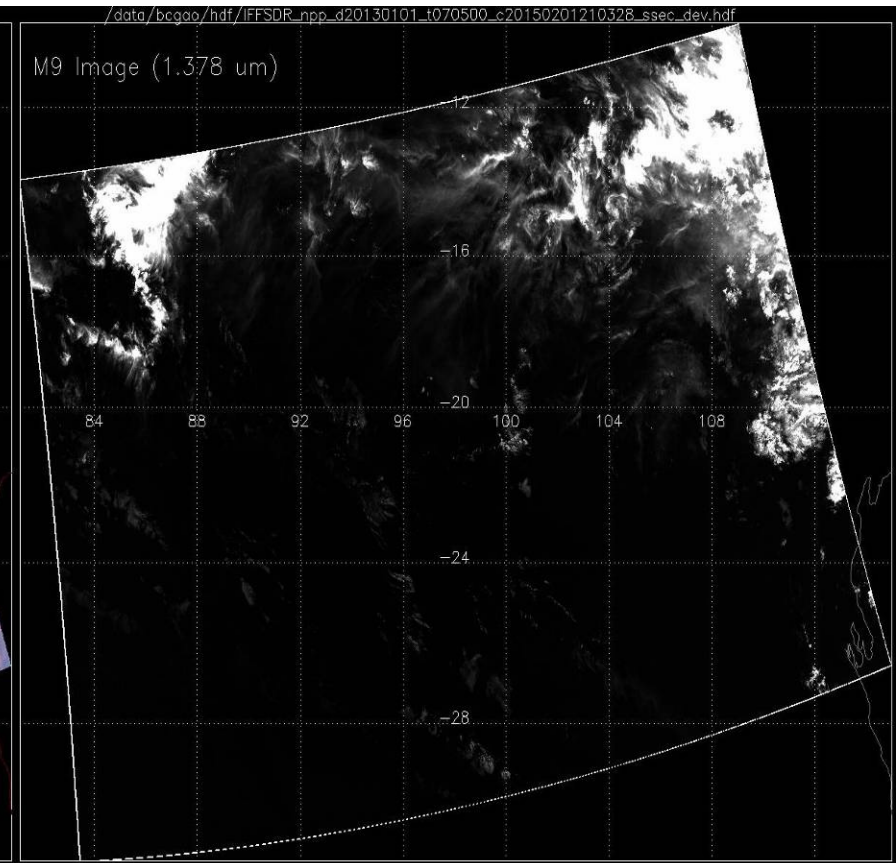and M1 at the beginning of the scan but is still less than the 3% sensor specification (i.e., see Table II for specification values per band). The polarization sensitivity tends to be highly variable across the scan; the highest levels of polarized light on orbit are expected at the end of the scan for the S-NPP orbit. In addition, the polarization factors were observed to be detector dependent. At present, the root cause of this dependence has not been identified. In conclusion, the prelaunch polarization testing has shown that the VIIRS VisNIR bands are compliant with the polarization factor requirement with a significant margin, and the uncertainty of the derived polarization factors was less than the characterization uncertainty specification of 0.5%.

Based on these polarization measurement figures and the repeatability of the measurements (0.15%), one can expect that differential polarizations can contribute to the striping in VIIRS images.

18

An Example of VIIRS Images Over Sunglint Regions

VIIRS RGB Image   VIIRS M9 Image

An Example of VIIRS Images Over Desert & Red Sea

VIIRS RGB Image

VIIRS M9 Image